



Multi-model dynamic climate emulator for solar geoengineering

Douglas G. MacMartin¹ and Ben Kravitz²

¹Department of Mechanical and Aerospace Engineering, Cornell University, Ithaca NY, USA and Computing + Mathematical Sciences, California Institute of Technology, Pasadena CA, USA

²Atmospheric Sciences and Global Change Division, Pacific Northwest National Laboratory, Richland, WA, USA

Correspondence to: D. G. MacMartin (dgm224@cornell.edu)

Abstract. Climate emulators trained on existing simulations can be used to project the climate effects that would result from different possible future pathways of anthropogenic forcing, without relying on general circulation model (GCM) simulations for every possible pathway. We extend this idea to include different amounts of solar geoengineering in addition to different pathways of greenhouse gas concentrations by training emulators from a multi-model ensemble of simulations from the Geoengineering Model Intercomparison Project (GeoMIP). The emulator is trained on the abrupt $4\times\text{CO}_2$ and a compensating solar reduction simulation (G1), and evaluated by comparing predictions against a simulated 1% per year CO_2 increase and a similarly smaller solar reduction (G2). We find reasonable agreement in most models for predicting changes in temperature and precipitation (including regional effects), and annual-mean Northern hemisphere sea ice extent, with the difference between simulation and prediction typically smaller than natural variability. This verifies that the linearity assumption used in constructing the emulator is sufficient for these variables over the range of forcing considered. Annual-minimum Northern hemisphere sea ice extent is less-well predicted, indicating the limits of the linearity assumption. For future pathways involving relatively small forcing from solar geoengineering, the errors introduced from nonlinear effects may be smaller than the uncertainty due to natural variability, and the emulator prediction may be a more accurate estimate of the forced component of the models' response than an actual simulation would be.

1 Introduction

Climate emulators have been used extensively to provide projections of climate changes for different anthropogenic forcing trajectories. These are trained based on a limited number of simulations with General Circulation Models (GCMs) and allow interpolation of climate response for a much broader set of trajectories, trading the fidelity of a GCM simulation for computational efficiency. A similar approach could in principle be undertaken for projections of the climate effects from solar geoengineering. Various solar geoengineering approaches have been suggested for intentionally in-



25 fluencing Earth's radiation budget, such as the injection of aerosols into the stratosphere (see, e.g.,
National Academy of Sciences, 2015). It is possible that such approaches may be considered in
the future for reducing some amount of climate damages. However, any climate model simulation
of geoengineering necessarily corresponds to some specific scenario, such as offsetting all of the
global-mean-temperature change from other anthropogenic forcing, (as in GeoMIP; Kravitz et al.,
30 2011). It is therefore useful to develop emulators that can use existing simulations in order to pre-
dict climate consequences both for different future trajectories of greenhouse gas forcing and for
different possible choices regarding the level of geoengineering.

The simplest emulator approach is pattern scaling (Santer et al., 1990; Mitchell, 2003; Tebaldi
and Arblaster, 2014), where a predictive dynamic model is used only for the time-evolution of the
35 global mean temperature (either from energy balance approaches or estimated directly from GCM
simulations), and the temperature at every spatial location is assumed to vary with the same time
evolution as the global mean – that is, that the pattern of temperature change is not itself a function
of time. Other variables, such as precipitation changes, are also assumed to scale with the global
mean temperature, so that the only “memory” in the emulator is embedded in the dynamics of the
40 global mean temperature response. Of course, not all of the climate system responds to forcing with
the same time-constants. Pattern scaling can be improved upon by introducing additional dynamic
variables, such as land-sea temperature contrast (Joshi et al., 2013), multiple empirical orthogonal
functions (EOFs) of temperature (Holden and Edwards, 2010; Herger et al., 2015), or by including
many more spatial degrees of freedom to better predict regional effects (Castruccio et al., 2014).
45 Additional spatial patterns can also be included to capture other forcing agents including aerosols
(Schlesinger et al., 2000; Frieler et al., 2012). Cao et al. (2015) include the climate response to a
solar reduction in a dynamic emulator, with global-mean-temperature as the sole dynamic predictor
(in addition to instantaneous forcing). The use of only one or a few dynamic variables (or predictors)
is ultimately constrained by the difficulty in estimating the dynamic response of additional variables
50 in the presence of climate variability due to low signal-to-noise ratio.

The primary assumption typically made in developing a climate emulator is that the climate re-
sponse is sufficiently linear and time-invariant (LTI). (We are explicit about our usage of the terms
linear and *non-linear* in Section 2 below.) Success with emulators illustrates that linearity can be a
reasonable approximation, although the accuracy of this assumption will depend on the variable and
55 the level of applied forcing (e.g., Tebaldi and Arblaster, 2014). The response of any LTI system to
any time-varying forcing can be described by a convolution between the impulse response function
that describes the system dynamics and the exogenous forcing; see equation (1) in Section 2 below,
and also Åström and Murray (2008, Sec. 5.3) or Ragone et al. (2015, eq. 2). “Training” the emulator
amounts to estimating the impulse response from one or more simulations.

60 We start from the same LTI assumption here as in the references above, but extended to include
solar geoengineering. The spatial patterns of the responses to solar and greenhouse gas forcing will



not be the same, leading to regional differences in outcomes (Ricke et al., 2010; Kravitz et al., 2014, 2015), nor are the precipitation responses the same (Bala et al., 2010), nor necessarily the time-
evolution of the responses (Cao et al., 2015). All of these factors are important to capture if the
65 emulator is to be useful in understanding climate effects of strategies that include solar geoengineer-
ing. We therefore do not start with any *a priori* assumptions on the form of the dynamics, and begin
by considering independent predictors for each variable. For estimating the spatial temperature and
precipitation response, we employ an EOF-based approach (as in Herger et al., 2015) with a common
set of EOFs constructed from both CO₂-forced and geoengineering simulations. In addition to tem-
70 perature and precipitation, we also consider Northern hemisphere sea-ice extent (see Supplementary
Material for net primary productivity; NPP).

We use simulations from the Geoengineering Model Intercomparison Study (GeoMIP, Kravitz
et al., 2011) where solar reduction is used as a proxy for any approach that reduces incoming short-
wave radiation. By training the emulator on one set of simulations and validating on a second, we
75 can evaluate the fundamental assumption of linearity. Section 2 describes the methodology and sim-
ulations used, and the resulting emulator and validation are given in Section 3.

2 Approach

The expectation that an emulator calibrated to match the GCM response to one climate forcing path-
way can also do so for a different pathway is typically based on the assumption that the response to
80 forcing can be reasonably approximated as linear and time-invariant (LTI). Consider a system forced
by both time-dependent forcing $f(t)$ from changes in atmospheric greenhouse gas concentrations
and time-dependent forcing $g(t)$ from solar geoengineering. For any variable $z_i(t)$, define $z_i^f(t)$ as
the response to forcing $f(t)$ with $g(t) = 0$ and $z_i^g(t)$ as the response to forcing $g(t)$ with $f(t) = 0$,
where the response is defined in each case as the difference relative to the initial state, and neglect-
85 ing natural variability. The system is *linear* if for any scalars α and β , the response to the combined
forcing $\alpha f(t) + \beta g(t)$ is the same linear combination of the individual responses, $\alpha z_i^f(t) + \beta z_i^g(t)$.
Note that in general, even if the system is linear, the ratio of any two variables will vary with time
simply because different variables respond at different rates; that is, for any forcing scenario, there
is not in general some constant μ such that $z_i(t) = \mu z_j(t)$ for all time (a plot of $z_i(t)$ against $z_j(t)$
90 will not be a straight line if these variables respond with different time constants). The usage of the
word nonlinear to express this latter idea is distinct from the concept of the dynamic system itself
being linear or nonlinear. By a dynamic system we simply mean that $z(t)$ depends on past values of
the forcing $f(t)$ or $g(t)$ in addition to the current values. A linear system can be characterized purely
by its response to a Dirac delta function; this is the *impulse response*.

95 For an LTI system forced by both time-dependent $f(t)$ and $g(t)$, the response of any variable $z_i(t)$
can be expressed in terms of a convolution between the input time-series and the system impulse



response functions as

$$z_i(t) = \int_0^t h_i^f(\tau) f(t-\tau) d\tau + \int_0^t h_i^g(\tau) g(t-\tau) d\tau + n_i(t) \quad (1)$$

where $h_i^f(t)$ is the impulse response due to greenhouse gas forcing and $h_i^g(t)$ the impulse response due to solar reductions; these will not in general be identical, nor in general the same for any choice of output variable z_i . The variable $n_i(t)$ is included to denote climate variability. The system is time-invariant if $h(\tau)$ in equation (1) does not depend explicitly on the current time t ; some possible exceptions are noted in Section 4. Herein we consider only annual-mean variables. The same formalism as in equation (1) also applies for predicting the seasonal-dependence of the response of a linear (but time-periodic) system, where the impulse response in general also depends on the time of year (e.g., $h = h(\tau, m)$ for month m) and additional training simulations would be required to estimate the seasonal-dependence of h . If the climate system were indeed LTI, then equation (1) would hold for any variable (temperature, precipitation, etc) either at any one location or projected onto any particular spatial pattern.

To estimate the impulse response for CO₂ forcing, we use the difference between the abrupt 4×CO₂ simulation and pre-industrial simulation for each of the models participating in GeoMIP. To estimate the impulse response for solar reduction, we use the G1 simulation from GeoMIP, in which the CO₂ concentration was quadrupled and insolation decreased to approximately maintain radiative balance and hence global mean temperature (see Figure S1). The difference between G1 and the 4×CO₂ simulations thus gives the response to an abrupt change in solar forcing. Note that each model separately chose the level of solar reduction $g_{4\times}$ required to balance the forcing from increased atmospheric CO₂, so that the percent solar reduction in G1 varies from model to model based on the efficacy of solar forcing in that model; see Table S1. Define

$$f(t) = \log_2 \left(\frac{\text{CO}_2(t)}{\text{CO}_{2,\text{ref}}} \right) \div 2 \quad (2)$$

$$g(t) = - \left(\frac{\text{Solar}(t) - \text{Solar}_{\text{ref}}}{\text{Solar}_{\text{ref}}} \right) \div g_{4\times} \quad (3)$$

where CO₂(t) is the time-varying atmospheric CO₂ concentration and Solar(t) is the solar irradiance. The 4×CO₂ experiment then corresponds to forcing $f(t) = 1, t \geq 0$ and $f(t) = 0, t < 0$ with $g(t) = 0$, while the GeoMIP G1 simulation uses the same $f(t)$ but with $g(t) = 1, t \geq 0$.

Substituting into Equation (1) then for any variable $z_i(t)$, the difference $z_i^{4\times}(t)$ between its value in 4×CO₂ and preindustrial is given by

$$z_i^{4\times}(t) = \int_0^t h_i^f(\tau) d\tau + n_i(t) \quad (4)$$



and the difference $z_i^{G1}(t)$ between its value in G1 relative to $4\times\text{CO}_2$ is

$$125 \quad z_i^{G1}(t) = \int_0^t h_i^g(\tau) d\tau + n_i(t) \quad (5)$$

from which we can estimate

$$\hat{h}_i^f(t) = \frac{d}{dt} z_i^{A\times}(t) \quad \text{and} \quad \hat{h}_i^g(t) = \frac{d}{dt} z_i^{G1}(t) \quad (6)$$

The impulse responses $h_i^{f,g}(t)$ could be estimated from the time-series of any forced simulation, but take particularly simple form from these step response simulations. (A linearly increasing forcing scenario such as a 1% per year increase in CO_2 also leads to a simple form, with the impulse response

130 proportional to the second derivative of the 1% CO_2 response.)

These impulse response estimates are “noisy” due to natural variability. Various approaches could be used to reduce the influence of natural variability, such as

1. Using multiple ensemble members or multiple forcing scenarios (as in Castruccio et al., 2014, for example),
- 135 2. Only considering spatial averages by computing the global mean as in pattern scaling, projecting onto EOFs as in Herger et al. (2015), or averaging over specific spatial regions as in Castruccio et al. (2014),
3. Applying temporal filtering to smooth high-frequency noise in \hat{h} or fitting $h(t)$ to some estimated functional form such as semi-infinite diffusion for global mean temperature (Caldeira and Myhrvold, 2013) or a multiple-exponential (Castruccio et al., 2014) or
- 140 4. Finding some less-noisy predictive variable, such as global mean temperature, to use as the predictor of other, noisier variables (effectively what is done in predicting the regional precipitation or temperature response in any pattern scaling analysis).

Choosing simulations with high forcing levels to train the emulator ($4\times\text{CO}_2$ and GeoMIP G1) 145 allows us to make useful predictions at lower forcing levels without the need for introducing arbitrary a priori assumptions on the functional form of the dynamics, such as that every field simply scales with global mean temperature. The penalty for this choice is that the high forcing will exacerbate any nonlinear effects; this precludes, for example, useful predictions of the Northern hemisphere annual-minimum sea ice extent, which would require that a lower-forcing simulation be used to train the 150 emulator.

A frequency-domain perspective is useful to understand how the “noise” due to climate variability affects the emulator predictions. The Laplace transform of Equation (1) transforms the convolution into multiplication:

$$\mathcal{L}(z_i) = \mathcal{L}(h_i^f) \mathcal{L}(f) + \mathcal{L}(h_i^g) \mathcal{L}(g) + \mathcal{L}(n_i) \quad (7)$$

$$155 \quad = H_i^f(s) F(s) + H_i^g(s) G(s) + N(s) \quad (8)$$



where the Laplace transform of the impulse response, $H_i(s) = \mathcal{L}(h_i)$, is the *transfer function* between that input and that output; capital letters will denote the Laplace transform of $h(t)$, $f(t)$ and $g(t)$. The impulse response could thus equivalently be estimated by first taking the Laplace transform of the input and output, computing the ratio, and computing the inverse transform. Consider for
 160 example the response to increased CO₂ (the estimation for solar reduction is analogous), where the emulator is trained on the input $f_t(t)$ and used to predict the response to forcing $f_p(t)$, with Laplace transforms $F_t(s)$ and $F_p(s)$. The transfer function estimate used by the emulator is

$$\hat{H}_i^g(s) = H_i^f(s) + \frac{N(s)}{F_t(s)} \quad (9)$$

and hence in the frequency domain the response predicted by the emulator for input forcing $F_p(s)$ is
 165

$$\hat{Z}_i = Z_i(s) + N(s) \frac{F_p(s)}{F_t(s)} \quad (10)$$

That is, climate variability in the simulation used to train the emulator leads to an error in the prediction that depends on the ratio of frequency content in the forcing signals between training and prediction simulations. Because a “step” change in the input such as in the abrupt 4×CO₂ simulation has more signal energy at low frequencies than high (Laplace transform proportional to $1/s$),
 170 it leads to a better estimate of the output response at low frequencies than at high frequencies; the high-frequency estimation errors due to natural variability manifest as “noise” on the estimated impulse response (see Figure 1 for an example). However, the smoothly varying radiative forcing input due to a 1% per year increase in CO₂ has even less energy at high temporal frequencies than the step
 175 input (Laplace transform proportional to $1/s^2$). Thus training an emulator on a “step” input simulation and then using it to predict the results from a smoothly-varying forcing trajectory will result in relatively noise-free emulator predictions, despite the apparent high-frequency “noise” in the impulse response. Note that the GeoMIP G2 simulation (described at the beginning of the next section) has an abrupt change in the solar forcing at year 50 (see Figure S1), and the emulated responses to
 180 this “step” change in forcing are, as expected, noisier than those due to the smooth forcing changes over the first 50 years of G2.

3 Results and validation

The impulse responses $h_i^f(t)$ and $h_i^g(t)$ are estimated for a number of different variables from the abrupt 4×CO₂ and G1 simulations as described above. The impulse-response based emulator for
 185 CO₂ forcing without any solar reduction can be validated by comparing the predictions with the simulations for a 1% per year increase in CO₂ (1%CO₂). To validate the emulation of solar reduction, we use the GeoMIP G2 scenario, in which CO₂ levels increase at 1% per year, and for the first 50 years, the solar reduction is gradually increased to balance this forcing. This uses the same ratio



of $g(t)$ to $f(t)$ as in G1 for each model. After 50 years, the solar reduction is returned to zero so
190 that only the radiative forcing from the CO₂ remains (see Kravitz et al. (2011) and Supplementary
Figure S1 for a schematic of the forcing in the G1 and G2 simulations). Several of the climate models
that conducted experiments G1 and G2 exhibit significant drift in the absence of net radiative forcing,
presumably due to initialization issues. These models are not considered further, leading to a total of
9 models considered here (Table S1).

195 The impulse response functions for predicting the global mean temperature and precipitation re-
sponses to either CO₂ or solar forcing are shown in Figure 1, averaged over all of these climate
models. As expected these are “noisy” estimates due to natural variability. Note that while the tem-
perature response characteristics are similar (aside from the sign) for increased CO₂ and reduced
insolation, the precipitation response differs. The impulse response of precipitation clearly high-
200 lights that CO₂ and solar reduction have different “fast” responses (rapid atmospheric adjustments
in the climate system before temperature has time to adjust) related to different amounts of radiative
forcing absorbed by the atmosphere (e.g., Andrews et al., 2010).

Figure 2 validates the ability of the impulse response formulation in equation (1) tuned from the
4×CO₂ and G1 simulations to correctly predict the global mean temperature response from the
205 1%CO₂ and G2 simulations. Figure 3 shows the corresponding plots for global mean precipitation.
Similar results are shown in the supplementary material (Figures S2–S3) for the temperature or pre-
cipitation difference between land and ocean. Linearity has previously been argued as a reasonable
assumption for temperature and precipitation responses (Kravitz et al., 2014, and references therein)
and since that is the only assumption made in constructing the emulator, this analysis also validates
210 that assumption for these variables and at these forcing levels. Note that the difference between
GCM-simulated and emulator-predicted trajectories is typically less than the standard deviation of
natural variability.

Northern hemisphere sea ice extent is an example of a variable that is both highly relevant for
assessing possible future scenarios, yet one in which a nonlinear response to forcing might be ex-
215 pected. The 4×CO₂ forcing is large enough that September sea ice is nearly lost in all models, and
thus an emulator trained off of this simulation will do a relatively poor job at predicting the reduction
in annual-minimum sea ice extent from smaller forcing. However, despite the obvious nonlinearity
in the annual-minimum extent, the annual-mean sea ice extent does behave sufficiently linearly in
most models, even at this large a forcing level, so that the 4×CO₂ simulation can be used to train a
220 useful emulator. This is illustrated in Figure 4.

Finally, Figure 5 illustrates the ability to capture the spatial response. One of the concerns raised
regarding the use of solar geoengineering is that the response from turning down the sun does not
perfectly compensate that from increased CO₂, resulting in some regional differences in temperature
and precipitation responses (Ricke et al., 2010; Kravitz et al., 2014). It is therefore valuable to assess
225 whether the emulator can capture some of the regional variation in the response between CO₂ and so-

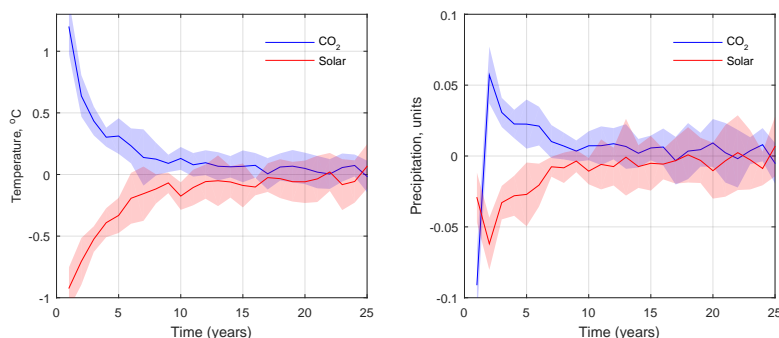


Figure 1. Estimated impulse response for CO₂ and solar forcing, for global mean temperature and precipitation, averaged over all 9 models (table S1); the inter-model standard deviation is shown by the shaded bands. While these impulse response functions are “noisy”, predictions made using them are less so, particularly for forcing levels much smaller than those used in estimating these functions. Note for precipitation the robust “fast” response to increased CO₂ has the opposite sign as the “slow” response.

lar forcing. For each model, EOFs are constructed from the spatial temperature response using both $4\times\text{CO}_2$ and G1 simulations to construct a single set of combined EOFs. In general, only the first few principal components are distinguishable from climate variability and have any predictive capability (Figure S4). Figure 5 plots the model-mean temperature and precipitation responses averaged over
230 years 41-50 of the G2 simulation for both the simulation and the emulator prediction. Note that only after averaging over 10 years and 9 climate models are the temperature and precipitation changes due to G2 – which is designed to have near-zero top-of-atmosphere radiative forcing – statistically significant at the grid-cell level. The differences here between the simulated and emulated responses are not significant at the grid cell level, although greater spatial averaging may indicate some statistically significant regional differences. In particular, the emulator appears to slightly underpredict
235 the amount of residual Arctic warming in G2, likely due to the nonlinearity associated with sea ice albedo feedback at the $4\times\text{CO}_2$ forcing used in training the emulator. Beyond this feature, it is difficult to assess with certainty to what extent the differences between the simulated and emulated regional responses are due to nonlinearities or simply due to natural variability. There is no evidence
240 of nonlinearity in either the ability of the emulator to capture differences between land and ocean temperatures or precipitation (Figure S2 and S3), nor in capturing the first few principal components of the response (Figure S4). Because the emulated response is based on simulations with roughly three times higher radiative forcing, and because the process of its construction suppresses high-frequency natural variability, it is potentially a more accurate representation of the forced-response
245 to G2 in the models than that obtained from the actual G2 simulation.

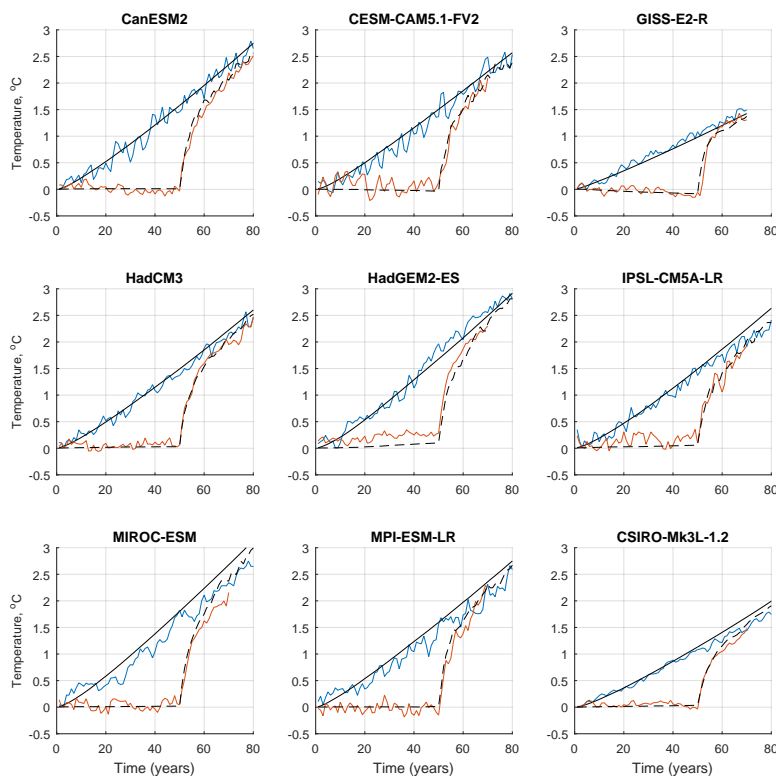


Figure 2. Simulated and predicted global mean temperature, both for a 1% per year increase in CO₂ (blue curves) and for GeoMIP experiment G2 (red), for each of the climate models considered here. The predicted response using the emulator is given by black lines, solid for the 1% CO₂ case and dashed for G2.

4 Discussion

Climate emulators provide a powerful tool for assessing any proposed future pathway of mitigation choices (including carbon dioxide removal) and different levels of geoengineering. For example, solar geoengineering could be used only to limit peak warming as part of an “overshoot” scenario in which atmospheric CO₂ concentrations peak and subsequently decline as net-negative carbon emissions reduce concentrations (Long and Shepherd, 2014; Tilmes et al., 2016). A limited, temporary deployment has also been described as a way to reduce the rate of warming (Keith and MacMartin, 2015; MacMartin et al., 2014). These types of limited-deployment scenarios are motivated in part by recognizing that solar geoengineering sufficient to reduce global mean temperature to preindustrial levels could lead to significant regional disparities and other risks, while a deployment that only partially reduces global mean temperature might decrease some metrics of climate change everywhere (Kravitz et al., 2014).

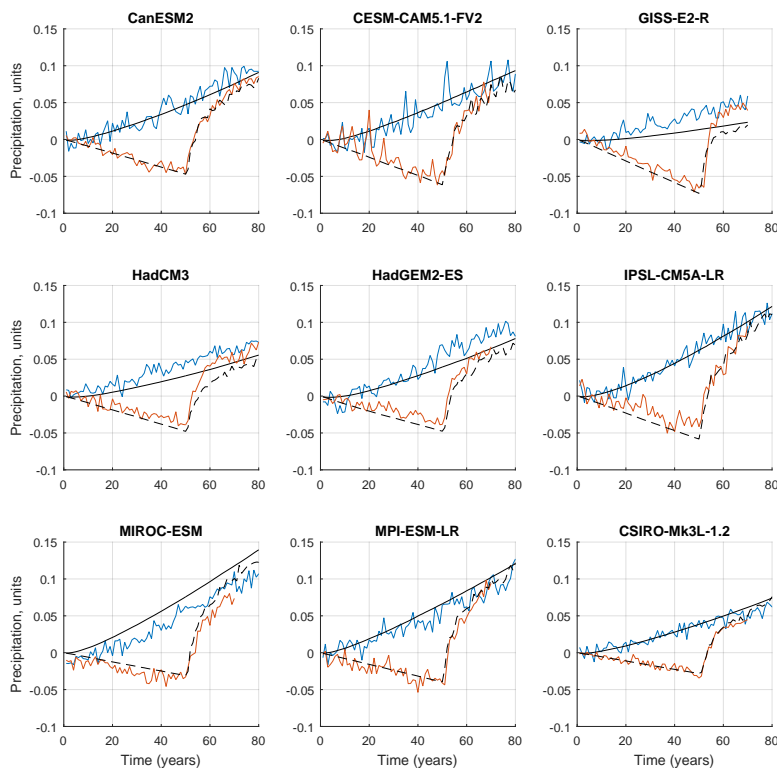


Figure 3. As in Figure 2 but for global mean precipitation. Simulated and emulated response are shown for 1% per year increase in CO₂ and GeoMIP experiment G2 for each of the climate models considered here.

By training emulators on a standard set of simulations, such as GeoMIP, that have been conducted by multiple modeling centers, any future scenario such as these can be readily evaluated with
260 multiple models. This can provide more insight into the robustness of conclusions than detailed simulations with any single model. (Of course, any collection of models is an ensemble of opportunity, with interpretation challenges as a statistical sample; see, e.g., Collins et al. (2013), Section 12.2, for a thorough discussion.) The emulator used here assumes that the climate system response can be sufficiently well approximated over the range of forcing levels of interest by the output of a linear
265 system. For many variables, the analysis here indicates that this is a sufficiently good assumption, with the difference between simulated and emulated responses smaller than the standard deviation of natural variability. There are many more variables that may be of interest, including higher moments to predict extremes; similar analysis as here could be used to assess whether a linear assumption is or is not sufficient for projecting the response of any variable beyond those considered here.

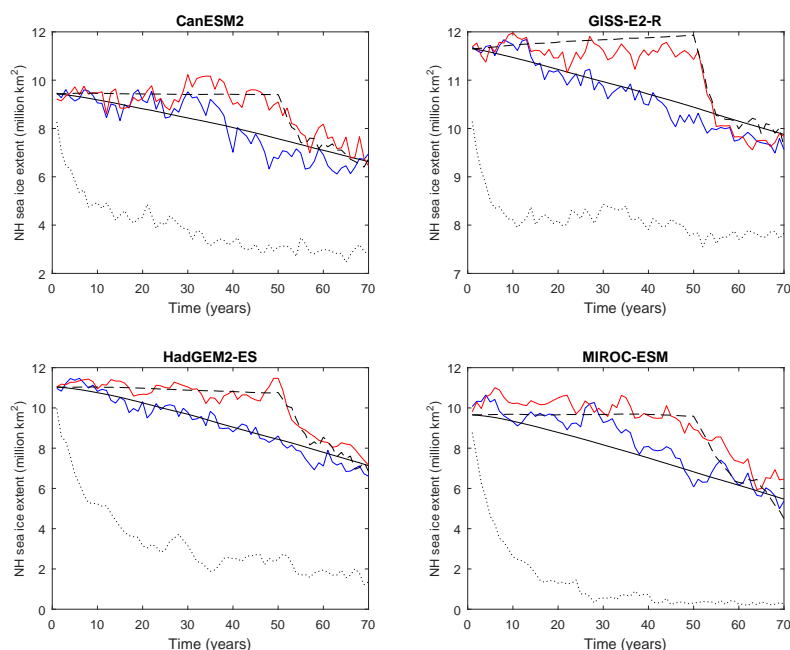


Figure 4. As in Figure 2 but for Northern Hemisphere annual-mean sea ice extent. Simulated and emulated response are shown for 1% per year increase in CO_2 and GeoMIP experiment G2 for several of the climate models considered here; the dotted line shows the response for the abrupt $4\times\text{CO}_2$ simulation.

270 Finally, note that the results herein were obtained using simulations that reduce the solar constant
as a proxy for any solar geoengineering approach. The climate effects from any specific technology,
such as stratospheric aerosol injection (SAI) will differ (e.g., Ferraro et al., 2015) both due to the dif-
ferent mechanism of radiative forcing, and the different spatial pattern of radiative forcing (the latter
being at least partially a design choice; Kravitz et al., 2016). Further, while linearity appears to be a
275 reasonable assumption in these climate models for predicting the response of many climate variables
to an imposed solar reduction, it may be a poorer approximation for SAI, for example. Nonlinearities
will occur in aerosol size distribution (Heckendorn et al., 2009; Niemeier and Timmreck, 2015), as
well as due to changes in the stratospheric circulation that result from the aerosols (Aquila et al.,
2014); time-invariance might also not hold if, for example, time-varying stratospheric chlorine con-
280 centrations (which affects the aerosol impact on ozone) are considered part of the “system” rather
than a forcing. It is unclear how significantly these will affect the ability to develop emulators for
this technology.

Author contributions. DGM and BK designed the study, conducted the analysis, and wrote the paper.

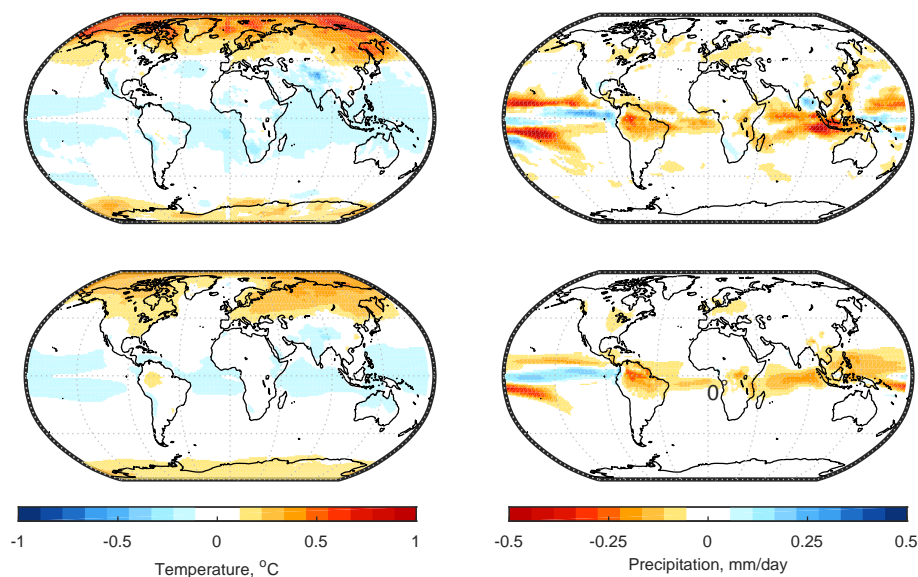


Figure 5. Temperature (left) and precipitation (right) averaged over years 41-50 of G2 simulation and averaged over all 9 models. The upper row shows the simulated results; the lower row shows the prediction based on a spatial emulator developed using 4 EOFs for each model. As noted elsewhere, the robust response to increasing CO_2 and reducing insolation to maintain zero global mean temperature difference is a net reduction (overcompensation) of global mean precipitation (Bala et al., 2010), and an overcooling of the tropics and an undercooling of the poles (Kravitz et al., 2013). The latter is an artifact of a latitudinally-uniform reduction in sunlight, and could be better managed by increasing the forcing at high latitudes relative to low (Kravitz et al., 2016).

Acknowledgements. We thank all participants of the Geoengineering Model Intercomparison Project and their model development teams, CLIVAR/WCRP Working Group on Coupled Modeling for endorsing GeoMIP and the scientists managing the Earth System Grid data nodes who have assisted with making GeoMIP output available. The Pacific Northwest National Laboratory is operated for the U.S. Department of Energy by Battelle Memorial Institute under contract DE-AC05-76RL01830. This work was partially supported by Cornell University's David R. Atkinson Center for a Sustainable Future (ACSF).



290 References

- Andrews, T., Forster, P. M., Boucher, O., Bellouin, N., and Jones, A.: Precipitation, radiative forcing and global temperature change, *Geophys. Res. Lett.*, 37, 2010.
- Aquila, V., Garfinkel, C. I., Newman, P. A., Oman, L. D., and Waugh, D. W.: Modifications of the quasi-biennial oscillation by a geoengineering perturbation of the stratospheric aerosol layer, *Geophys. Res. Lett.*, 41, 2014.
- 295 Åström, K. J. and Murray, R. M.: *Analysis and Design of Feedback Systems*, Princeton, 2008.
- Bala, G., Caldeira, K., and Nemani, R.: Fast versus slow response in climate change: implications for the global hydrological cycle, *Clim. Dyn.*, 35, 423–434, 2010.
- Caldeira, K. and Myhrvold, N.: Projections of the pace of warming following an abrupt increase in atmospheric carbon dioxide concentration, *Env. Res. Lett.*, 8, 2013.
- 300 Cao, L., Bala, G., Zheng, M., and Caldeira, K.: Fast and slow climate responses to CO₂ and solar forcing: A linear multivariate regression model characterizing transient climate change, *J. Geophys. Res. Atmos.*, 120, 12037–12053, 2015.
- Castruccio, S., McInerney, D. J., Stein, M. L., Crouch, F. L., Jacob, R. L., and Moyer, E. J.: Statistical Emulation of Climate Model Projections Based on Precomputed GCM Runs, *J. Climate*, 27, 1829–1844, 2014.
- 305 Collins, M., Knutti, R., Arblaster, J., Dufresne, J.-L., Fichet, T., Friedlingstein, P., Gao, X., Gutowski, W., Johns, T., Krinner, G., Shongwe, M., Tebaldi, C., Weaver, A., and Wehner, M.: Long-term Climate Change: Projections, Commitments and Irreversibility, in: *Climate Change 2013: The Physical Science Basis. Contribution of Working Group I to the Fifth Assessment Report of the Intergovernmental Panel on Climate Change*, edited by Stocker, T. F., Qin, D., Plattner, G.-K., Tignor, M., Allen, S., Boschung, J., Nauels, A., Xia, Y., Bex, V., and Midgley, P., Cambridge University Press, Cambridge, United Kingdom and New York, NY, USA, 2013.
- 310 Ferraro, A. J., Charlton-Perez, A. J., and Highwood, E. J.: Stratospheric dynamics and midlatitude jets under geoengineering with space mirrors and sulfate and titania aerosols, *J. Geophys. Res. A*, 120, 414–429, 2015.
- Frieler, K., Meinshausen, M., Mengel, M., Braun, N., and Hare, W.: A scaling approach to probabilistic assessment of regional climate change, *J. Climate*, 25, 3117–3144, 2012.
- 315 Heckendorn, P., Weisenstein, D., Fueglistaler, S., Luo, B. P., Rozanov, E., Schraner, M., Thomason, L. W., and Peter, T.: The impact of geoengineering aerosols on stratospheric temperature and ozone, *Env. Res. Lett.*, 4, 2009.
- Herger, N., Sanderson, B. M., and Knutti, R.: Improved pattern scaling approaches for the use in climate impact studies, *Geophys. Res. Lett.*, 42, 2015.
- 320 Holden, P. B. and Edwards, N. R.: Dimensionally reduced emulation of an AOGCM for application to integrated assessment modelling, *Geophys. Res. Lett.*, 37, 2010.
- Joshi, M. M., Turner, A. G., and Hope, C.: The use of land-sea warming contrast under climate change to improve impact metrics, *Clim. Change*, 117, 951–960, 2013.
- 325 Keith, D. W. and MacMartin, D. G.: A temporary, moderate and responsive scenario for solar geoengineering, *Nature Climate Change*, 5, 2015.
- Kravitz, B., Robock, A., Boucher, O., Schmidt, H., Taylor, K. E., Stenchikov, G., and Schulz, M.: The Geoengineering Model Intercomparison Project (GeoMIP), *Atm. Sci. Lett.*, 12, 162–167, 2011.



- Kravitz, B., Caldeira, K., Boucher, O., Robock, A., Rasch, P. J., , Alterskjær, K., Karam, D. B., Cole, J. N. S.,
330 Curry, C. L., Haywood, J. M., Irvine, P. J., Ji, D., Jones, A., Lunt, D. J., Kristjánsson, J. E., Moore, J.,
Niemeier, U., Schmidt, H., Schulz, M., Singh, B., Tilmes, S., Watanabe, S., Yang, S., and Yoon, J.-H.:
Climate model response from the Geoengineering Model Intercomparison Project (GeoMIP), *J. Geophys.*
Res., 118, 2013.
- Kravitz, B., MacMartin, D. G., Robock, A., Rasch, P. J., Ricke, K. L., Cole, J. N. S., Curry, C. L., Irvine, P. J.,
335 Ji, D., Keith, D. W., Kristjansson, J. E., Moore, J. C., Muri, H., Singh, B., Tilmes, S., Watanabe, S., Yang, S.,
and Yoon, J.-H.: A multi-model assessment of regional climate disparities caused by solar geoengineering,
Env. Res. Lett., 9, 074 013, 2014.
- Kravitz, B., MacMartin, D. G., Rasch, P. J., and Jarvis, A. J.: A new method of comparing forcing agents in
climate models, *J. Climate*, 28, 8203–8218, 2015.
- 340 Kravitz, B., MacMartin, D. G., Wang, H., and Rasch, P. J.: Geoengineering as a Design Problem, *Earth Systems*
Dynamics, 7, 469–497, 2016.
- Long, J. C. S. and Shepherd, J. G.: The strategic value of geoengineering research, *Global Environmental*
Change, 1, 2014.
- MacMartin, D. G., Caldeira, K., and Keith, D. W.: Solar geoengineering to limit rates of change, *Phil. Trans.*
345 *Royal Soc. A*, 372, 2014.
- Mitchell, T. D.: Pattern Scaling: An examination of the accuracy of the technique for describing future climates,
Climatic Change, 60, 217–242, 2003.
- National Academy of Sciences: Climate Intervention: Reflecting Sunlight to Cool Earth, The National
Academies Press, 500 Fifth St. NW, Washington DC 20001, 2015.
- 350 Niemeier, U. and Timmreck, C.: What is the limit of climate engineering by stratospheric injection of SO₂?,
Atmos. Chem. Phys., 15, 9129–9141, 2015.
- Ragone, F., Lucarini, V., and Lunkeit, F.: A new framework for climate sensitivity and prediction: a modelling
perspective, *Clim. Dyn.*, 2015.
- Ricke, K. L., Granger Morgan, M., and Allen, M. R.: Regional climate response to solar-radiation management,
355 *Nature Geoscience*, 3, 537–541, 2010.
- Santer, B. D., Wigley, T. M. L., Schlesinger, M. E., and Mitchell, J. F. B.: Developing climate scenarios from
equilibrium GCM results, Tech. rep., MPI Report Number 47, 1990.
- Schlesinger, M. E., Malyshev, S., Rozanov, E. V., Yang, F. L., Andronova, N. G., Vries, B. D., Grubler, A., Jiang,
K. J., Masui, T., Morita, T., Penner, J., Pepper, W., Sankovski, A., and Zhang, Y.: Geographical distribution
360 of temperature change for scenarios of greenhouse gas and sulfur dioxide emissions, *Technol. Forecast Soc.*
Change, 65, 167–193, 2000.
- Tebaldi, C. and Arblaster, J. M.: Pattern scaling: Its strengths and limitations, and an update on the latest model
simulations, *Climatic Change*, 122, 459–471, 2014.
- Tilmes, S., Sanderson, B. M., and O'Neill, B.: Climate impacts of geoengineering in a delayed mitigation
365 scenario, submitted, 2016.